19

Electrodynamic Coupling between Ganymede and the Jovian Ionosphere

BERTRAND BONFOND AND PHILIPPE ZARKA

19.1 INTRODUCTION

Having conductive interiors and/or ionospheres, the Galilean satellites are in electrodynamic interaction with the fast-rotating Jovian magnetic field and magnetosphere in which they are embedded. In the inner Jovian magnetosphere, within the orbit of Ganymede, the magnetic pressure of the rotating flow is larger than its ram pressure (except in the near-equatorial current sheet at Ganymede's orbit) and the flow is sub-Alfvénic (Kivelson and Bagenal, 2014). The flow–obstacle interactions generate both local and distant effects. In this chapter, we do not focus on the local interaction, which is covered in Chapter 3.1 (Kivelson); rather we will zoom out and explore the outcome of this interaction further down the disturbed magnetic field lines. There, the electrodynamic satellite–Jupiter interaction takes the form of transverse perturbations of the Jovian magnetic field propagating away from the satellite along Jovian magnetic field lines at the Alfvén velocity, in both hemispheres, down to the Jovian ionosphere. These perturbations are called Alfvén waves and their envelopes Alfvén wings, primarily theorized by Neubauer (1980, 1998).

As these waves propagate along the magnetic field lines, they initiate a long chain of processes and generate a variety of signatures associated with the long-range interaction, as summarized in Figure 19.1. Some of them, noted in white, have already been observed at Ganymede, while others are expected to take place because they have been identified at Io (in cyan). Ganymede's magnetosphere forms a large obstacle for Jupiter's magnetospheric plasma and magnetic field rotating with the planet. Its motion relative to the plasma launches large-scale Alfvén waves, which then undergo some turbulent filamentation, and partial reflections at the Alfvén velocity gradients (either at the plasma sheet boundary or at the Jovian ionosphere). These waves ultimately enter a regime (mostly inertial Alfvén waves) in which they can accelerate charged particles (Section 19.4). Part of them hit the atmosphere, exciting and ionizing neutral atoms and molecules, which generates specific auroral emissions, called the Ganymede footprint (Section 19.2), as they de-excite. Another part of the accelerated electrons bounces due to the magnetic mirror effect. The resulting upgoing electron distribution is far from Maxwellian, as it lacks the electrons with small pitch angle which have precipitated into the atmosphere, causing the feature called a loss-cone in the velocity space ($v_\parallel$, $v_\perp$). This feature notably displays a positive gradient of the electron distribution function (or phase space density f($v_\parallel$, $v_\perp$)) towards increasing perpendicular velocities $v_\perp$. This positive gradient is the free energy source of the Cyclotron-Maser Instability (CMI) mechanism (Zarka, 1998; Hess, Mottez and Zarka, 2007; Hess et al., 2008), through which the perpendicular energy of electrons in cyclotron motion around the magnetic field lines is directly and collectively transferred to electromagnetic radio waves having this same cyclotron frequency ($f_{ce} = eB/2\pi m_e$). The corresponding electrons are said to be *resonant* and the wave is hugely amplified, either causing the electron distribution to relax towards a Maxwellian one, or trapping resonant electrons in the wave electric field, and in both cases quenching the instability (Le Quéau, 1988). Radio emissions are further detailed in Section 19.3.

Because Io is closer to Jupiter, where the magnetic field magnitude is larger than at Ganymede (∼2 000 nT at Io compared to ∼100 nT at Ganymede), and embedded into the dense plasma torus stemming from the moon's outstanding volcanism, all the outcomes of the moon–magnetosphere interaction are magnified there. Hence many of the phenomena related to the moon–magnetosphere interactions were first unveiled at Io before they were found to be also applicable at Ganymede. These distant consequences are key to studying these interactions because they often are the only way to get information in absence of a spacecraft directly measuring the local environment.

For example, it was the intense radio emissions related to Io that first revealed that this moon was playing such an important role in the Jovian magnetosphere. Over half a century ago, Bigg (1964) noticed that the recently discovered and variable Jovian decametre (DAM) radio emission showed maximum occurrence at specific orbital phases of Io (Φ_{Io}) around Jupiter as seen from a terrestrial observer (∼90° and ∼240° from the anti-observer's position – Figures 19.3a and 19.2b,c).

The picture grew in complexity as spacecraft brought new pieces of information on the Jovian system, starting from the simpler unipolar inductor model (Goldreich and Lynden-Bell, 1969), to the Alfvén wing theory (Neubauer, 1980) and then all its subsequent developments, involving the propagation and reflections of the Alfvén waves (Gurnett and Goertz, 1981; Jacobsen et al., 2007, 2010; Hinton et al., 2019), their turbulent filamentation (Chust et al., 2005), or their capability to accelerate particles (Jones and Su, 2008; Hess et al., 2010, 2013; Damiano et al., 2019).

The arrival of Juno around Jupiter and the traversal of the field lines connected to the Io footprint at high latitude offered a brand new perspective on the richness of the wave–particle interactions resulting from the moon–magnetosphere

https://doi.org/10.1017/9781108966474.020 Published online by Cambridge University Press

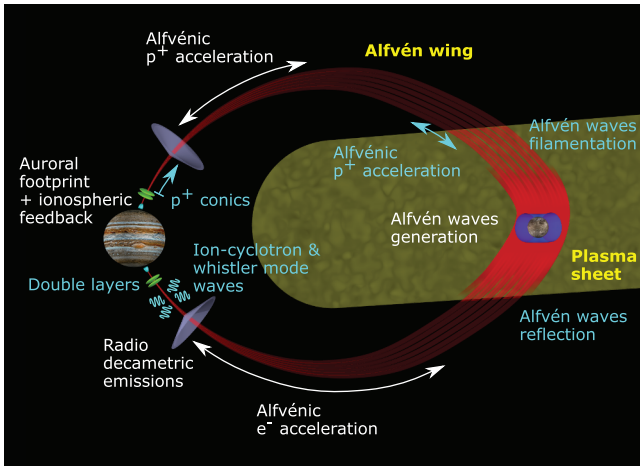

Figure 19.1 Schematic of the chain of processes taking place along the Alfvén wings (in red) generated by the interaction between the magnetosphere of Ganymede (in blue, not to scale) and that of Jupiter. The processes noted in white have already been observed at Ganymede and are the subject of the present chapter, while those noted in cyan have not been discovered yet, but are expected to exist because they have already been detected at Io.

couplings. The importance of Alfvén waves undergoing a turbulent cascade and accelerating electrons along the magnetic field lines through a broad range of energies was confirmed by in situ particle and electromagnetic wave observations (Szalay et al., 2018; Sulaiman et al., 2020). However, a greater surprise came from the finding of proton beams and conics, originating from three different regions along the Alfvén wing (Szalay et al., 2020a; Clark et al., 2020). Finally, ion-cyclotron waves and whistler-mode waves excited by the field-aligned electrons are also observed (Sulaiman et al., 2020).

An important question arose, however. Were these phenomena specific to Io's case, since this moon is the most volcanically active body of the solar system and the main source of material in the magnetosphere, or could they be extended to other moons, such as Europa and its induced magnetosphere related to its sub-surface ocean or – and this is the focus of our present interest – to Ganymede and its permanent intrinsic magnetic field.

Io lacks a permanent magnetic dipole. So, its non-local interaction with the Jovian magnetic field consists of (1) its steady Alfvén wings, which result from the stacking of Jupiter's magnetic field upstream of Io and its subsequent deflection around the satellite (Saur et al., 2004), and (2) a dense plasma wake that is rapidly re-accelerated downstream (Hinson et al., 1998).

The existence of an intrinsic magnetic field implies some modifications of this picture for Ganymede (Chapter 3.1). The obstacle in Jupiter's rotating magnetic field is not Ganymede's body or ionosphere but its magnetosphere, which is of 2–3 R_G radius (R_G stands for Ganymede's radius, ~2 634 km). The orientation of Ganymede's internal field, antiparallel to Jupiter's, leads to a favourable orientation of interacting magnetic fields resulting in reconnection at Ganymede's upstream and downstream magnetopauses and subsequent particle energization. A signature of this reconnection is the double loss-cone distributions (i.e. in both directions along the field line) observed by Galileo on magnetic field lines connected to both Ganymede and Jupiter (Williams et al., 1997). At high energies (keV–tens of keV), particles can bounce several times between mirror points close to Ganymede and close to Jupiter before the magnetic field line drifts across Ganymede's magnetosphere, and then be temporarily trapped and exhibit double loss-cone distributions, whereas at low energies, the larger pitch angle diffusion fills the loss-cones at some distance from the mirror points (Williams and Mauk, 1997).

The plasma energized by magnetic reconnection at the magnetopause also generates local electrostatic and electromagnetic emissions (Gurnett et al., 1996; Kurth et al., 2000). It is much more developed than at Io, as described in chapter 14.

Beyond a few R_G downstream of Ganymede, one finds Alfvén wings similar to Io's (Jia et al., 2008) as well as an extended plasma wake (Kivelson et al., 1998). The Alfvén wings carry a current of about 0.5 MA (Lavrukhin and Alexeev, 2015) driven by a transverse electric potential drop of about 80 kV across Ganymede's magnetosphere (Zhou et al., 2020) (versus a current ~1 MA driven by a 400 kV potential drop across Io's ionosphere). The Alfvén wings' field-aligned currents close in Ganymede's and Jupiter's ionospheres and in Ganymede's magnetotail or plasma wake (Jia et al., 2008).

For solar wind–planet interactions, the energy release is often sporadic (substorms) as a result of the variable character of the Solar wind and of magnetic flux storage in the magnetotail. But at Ganymede, immersed in Jupiter's magnetosphere, the upstream magnetic field conditions are essentially steady, with a slowly rocking orientation of the magnetic field external to Ganymede's magnetosphere. As a consequence, steady reconnection was anticipated at Ganymede's magnetopause, not a bursty, substorm-like one (Kivelson et al., 2004). These expectations were challenged by the reanalysis of Galileo plasma data recorded near Ganymede, showing plasma flows accelerated by time-variable magnetic reconnection consistent with Dungey-type substorms (Collinson et al., 2018).

Another source of variability of the interaction comes from the fact that Ganymede does not orbit permanently in a dense plasma environment like Io in its torus, but it periodically crosses the Jovian plasma sheet. Its plasma environment is thus very variable and induces a variable travel time of the Alfvénic perturbations between Ganymede and Jupiter. Bonfond et al. (2013) found a maximum longitudinal shift of 13° between the multiple spots of the Ganymede northern UV auroral footprint and Ganymede's instantaneous longitude, quite comparable to Io's lead angle up to ~15° in the north and ~8° in the south (Bonfond et al., 2017; Hinton et al., 2019).

19.2 AURORAL FOOTPRINTS

Discovery of the Ganymede Footprint

While the first detection of a satellite auroral footprint, Io's, took place in the infrared domain from a ground-based telescope (Connerney et al., 1993), all the subsequent first detections happened in the ultraviolet (UV) domain. The Europa and Ganymede footprints were first discovered with the Hubble Space Telescope (HST) (Clarke et al., 2002). Then came the discovery of the Enceladus footprint with the Ultraviolet Imaging Spectrograph (UVIS) on board Cassini (Pryor et al., 2011). Finally, a tentative identification of a Callisto footprint

https://doi.org/10.1017/9781108966474.020 Published online by Cambridge University Press

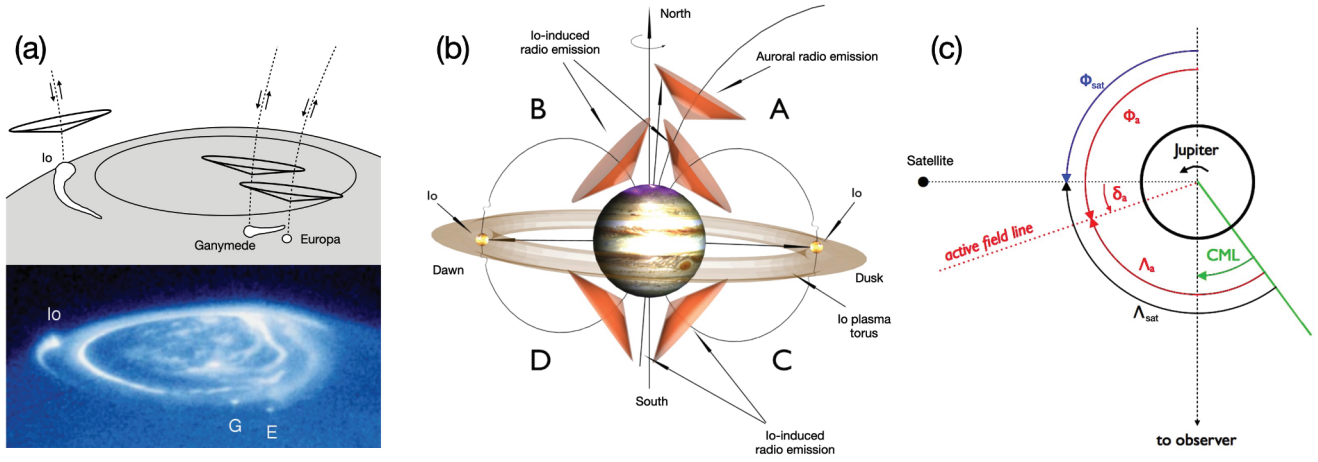

Figure 19.2 (a) Hubble Space Telescope UV image of northern Jovian auroral regions, showing the bright main auroral oval and the footprints of Io (and its tail-like, wake-induced emission), Ganymede, and Europa flux tubes. In the top part of the sketch, hollow conical beams of radio emission are displayed. They are produced above the UV hot spots by the energetic electrons precipitated along the satellite flux tubes or reflected upwards by magnetic mirroring. Similar radio emissions originate from sources distributed above the main oval. (b) Geometry and nomenclature of auroral and satellite-induced (here Io-induced) radio emissions. Radio emissions are produced along the displayed conical shells and thus are observable only when the source is near a limb of Jupiter. The magnetic field line connected to Io is sketched as the active, radio-emitting field line, but actually the active field line leads the instantaneous Io field line by several degrees (angle δ_a of panel (c)). (c) Definition of the different angles used to characterize the observing geometry. In green is the central meridian longitude (CML), which is the System III longitude of the observer. The satellite phase Φ_{sat} and its System III longitude Λ_{sat} are drawn in blue and black, respectively. Alfvén lead angle δ_a, phase, and phase Φ_a and longitude Λ_a of the so-called 'active' field line (in UV and radio) are shown in red. (a) From Clarke et al. (2002); Zarka (2007). Reprinted from *Planetary and Space Science*, 55(5). Philippe Zarka, Plasma interactions of exoplanets with their parent star and associated radio emissions, 598–617 ©2007, with permission from Elsevier. (b & c) From M. S. Marques, P. Zarka, E. Echer, V. B. Ryabov, M. V. Alves, L. Denis and A. Coffre, *A&A*, 604, A17, 2017, reproduced with permission © ESO.

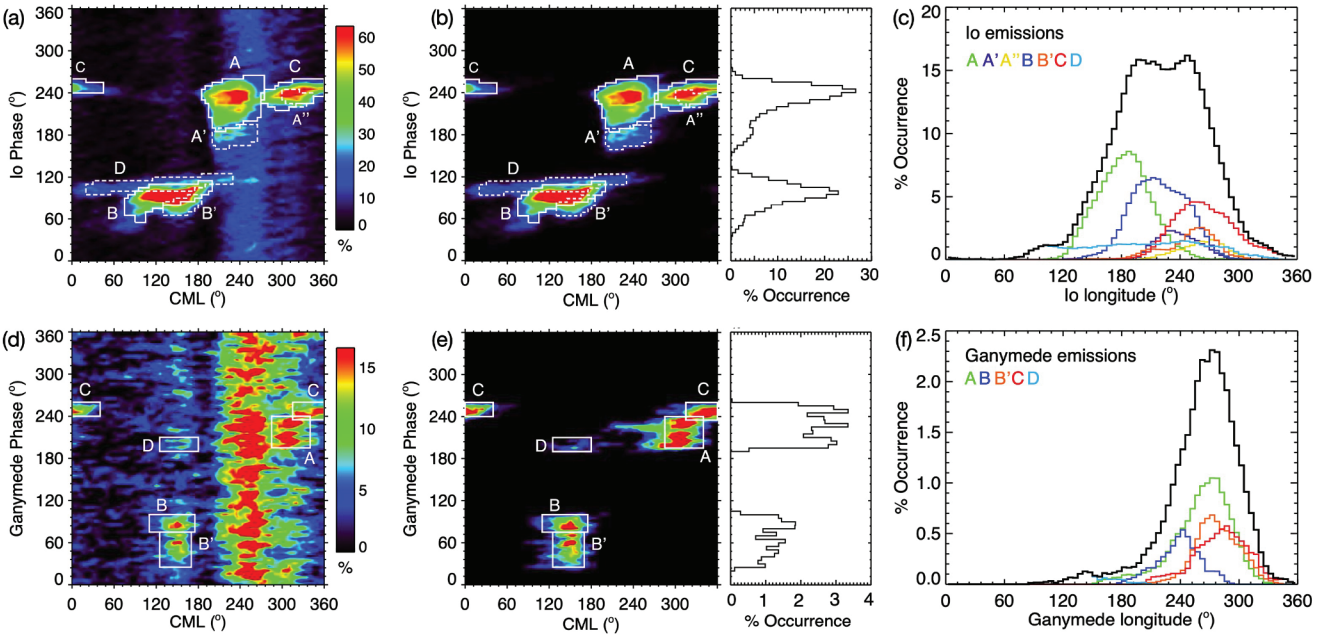

Figure 19.3 (a) Occurrence probability of Jovian radio emissions detected over 26 years (1990–2015) with the Nançay Decameter Array, displayed as 2D histograms as a function of planetary rotation (CML) and Io's orbital phase (Φ_{Io}) in 5° × 5° bins (smoothed via 1° interpolation). Regions of high occurrence labelled in white correspond to Io–Jupiter emissions (named Io-A, Io-B…). Vertical bands of emission covering restricted CML ranges at all Φ_{Io} correspond to non-Io emissions (auroral or induced by other satellites). (b) Occurrence probability of Io–Jupiter emissions only versus CML and Φ_{Io}. The profile integrated over all CML is displayed on the right-side panel. (c) Integrated occurrence probability of Io–Jupiter emissions versus Io's Jovicentric longitude ($\Lambda_{Io} = CML + 180° - \Phi_{Io}$). Components from panel (b) are identified by colours, and their sum is the black line. (d) Occurrence probability of non-Io emissions versus CML and Ganymede's orbital phase $\Phi_{Ganymede}$. Ganymede–Jupiter emissions show up within new regions of enhanced occurrence (white boxes), labelled A–D in reference to the non-Io components in which they have been identified. (e) Occurrence probability of Ganymede–Jupiter emissions only versus CML and $\Phi_{Ganymede}$. The profile integrated over all CML is displayed on the right-side panel. (f) Integrated occurrence probability of Ganymede–Jupiter emissions versus Ganymede's jovicentric longitude ($\Lambda_{Ganymede} = CML + 180° - \Phi_{Ganymede}$). Components from panel (e) are identified by colours, and their sum is the black line. From Zarka, P., Marques, M. S., Louis, C., Ryabov, V. B., Lamy, L., Echer, E. and Cecconi, B., *A&A*, 618, A84, 2018, reproduced with permission © ESO.

https://doi.org/10.1017/9781108966474.020 Published online by Cambridge University Press

was reported, based on HST UV images as well (Bhattacharyya et al., 2018). The Ganymede and Europa footprints have since also been identified in the infrared domain around 3.4 μm with the Jupiter InfraRed Auroral Mapper (JIRAM) camera on board Juno (Mura et al., 2017).

Both H and H_2 UV auroral emissions on one hand and H_3^+ infrared emissions on the other hand arise from the precipitation of charged particles into Jupiter's H and H_2 atmosphere. The UV emissions result from the de-excitation of atomic or molecular hydrogen after impact by precipitating particles (electrons or ions) or secondary electrons. Conversely, auroral infrared emissions are thermal emissions of H_3^+ ions which are themselves an indirect product of the electron precipitation followed by charge transfer (see review in Badman et al., 2015):

$$e^- + H_2 \rightarrow H_2^+ + 2e^-,$$
$$H_2^+ + H_2 \rightarrow H_3^+ + H.$$

Usually, H_3^+ emissions are observed around 3.4 μm because the strong absorption from CH_4 molecules located at lower altitude than most of the aurora offer a high contrast between the auroral emissions and the planetary background at this wavelength.

Morphology of the Ganymede Footprint

The first detections associated only one auroral spot with the Ganymede footprint (Clarke et al., 2002). On HST images, this spot can be fitted with an ellipse of area $\sim 5 \times 10^5$ km^2. When mapped back into the equatorial plane along magnetic field lines, such a surface corresponds to a disk with 8–20 times Ganymede's radius ($R_G = 2\,634$ km), thus corresponding to the size of Ganymede's magnetosphere rather than Ganymede itself (Grodent et al., 2009).

Using their characteristic motion on polar projections fixed in System III (the longitude system fixed with the magnetic field), it was found that, in some cases, at least two spots could be associated with the footprint of Ganymede (Bonfond et al., 2013) (Figure 19.4). The spacing between these two spots increases up to a maximum of about 4 000 km and then decreases systematically as a function of the position of Ganymede with respect to the plasma sheet, and they seem to merge when Ganymede is close to the central region of the sheet. This evolution of the inter-spot distances suggests that one spot corresponds to the main Alfvén wing (MAW) and the second one to the trans-hemispheric electron beam (TEB), that is, generated by electrons accelerated in the opposite hemisphere (see Figure 19.4 b).

The inter-spot distance also varies on timescales larger than Jupiter's rotation. Observations carried out in 2007 in similar Ganymede longitude ranges, but a few weeks apart, showed that this distance can vary by a factor of 2. Since the distance between spots is directly related to the Alfvén propagation time, such variations were attributed to an increase of plasma density in the Jovian magnetosphere that took place in the first month of 2007 (Bonfond et al., 2013). Indeed, several other observations, such as the brightening of Jupiter's sodium nebula (Yoneda et al., 2009), the decrease of the hectometric (HOM) radio emissions unrelated to the solar wind fluctuations (Yoneda et al., 2013), the increased occurrence rate of large plasma injection auroral signatures and the expansion of the main auroral oval over three months (Bonfond et al., 2012) all indirectly suggest that the plasma input from Io increased from February to June 2007.

In addition to the spots, an extended auroral tail ($\geq 24°$) can also sometimes be seen in the downstream direction along the Ganymede footpath (Bonfond et al., 2017). As with many features of the Ganymede footprint, this tail is harder to detect in UV images than Io's footprint tail. Moreover, even in similar geometrical configurations, the Ganymede footprint UV tail has only been identified in a handful of cases. These rare detections indicate that parameters other than just the position of Ganymede in the plasma sheet and the viewing geometry impact its apparent brightness (such as the plasma energy distribution, composition, density, the magnetic field strength, etc.). However, the existence of tails in both Ganymede's and Europa's footprints indicates that lessons learned from Io's footprint most likely also apply for the others and vice versa. Two main ideas have been proposed to explain the Io footprint tail. The first one involves a steady current loop related to the reacceleration of the stagnant plasma in Io's wake (Hill and Vasyliunas, 2002; Delamere et al., 2003; Su et al., 2003; Ergun et al., 2006; Matsuda et al., 2012), while the second involves the increasingly intricate reflection pattern of the Alfvén waves downstream of the satellite (Jacobsen et al., 2007; Bonfond et al., 2017). The broad energy distribution inferred from remote observations (Bonfond et al., 2009) and observed directly by Juno favours the second (Szalay et al., 2018). It is noteworthy that the existence of a footprint tail at Ganymede, where no significance mass loading takes place, indicates that this process is not a necessary ingredient to the formation of the tail.

Infrared observations from the JIRAM instrument on board Juno offer an unprecedented spatial resolution, down to 15 km/pixel (Mura et al., 2018; Moirano et al., 2021). They not only showed similar features in infrared H_3^+ emissions than in the UV, such as the pair of spots followed by the extended tail (Mura et al., 2017), but they also unveiled further details of the footprint morphology. In particular, and similarly to the Io footprint spots, each one of the two Ganymede footprint spots appears to be formed of a pair of smaller auroral dots separated by 170 km (Figure 19.4c) (Mura et al., 2018). One possible explanation is that these dots correspond to the front and tail of Ganymede's magnetosphere, where magnetic reconnection takes place. However, the presence of similar substructures at Io's footprint rather suggests another (and not mutually exclusive) origin, possibly related to Jupiter's ionosphere or to the electron acceleration process. This conclusion is further strengthened by the finding that the Ganymede footprint tail (as well as Io's and Europa's) was also made of sub-dots separated by ~270 km (Figure 19.4d). Contrary to the larger spots discussed earlier, these sub-dots appear fixed with the planet rather than following the motion of the satellite (Moirano et al., 2021). Because of this behaviour, as well as the size and spacing of the spots, Moirano et al. (2021) suggest that these features result from the ionosphere feedback instability, in which a localized increase of ionospheric conductivity in the presence of background ionospheric electric field enhances the ionospheric currents. In this scenario, the current enhancement closes through field-aligned currents at the conductivity gradient through secondary Alfvén waves, which further increases the precipitating electron flux and the conductivity, closing the feedback loop.

https://doi.org/10.1017/9781108966474.020 Published online by Cambridge University Press

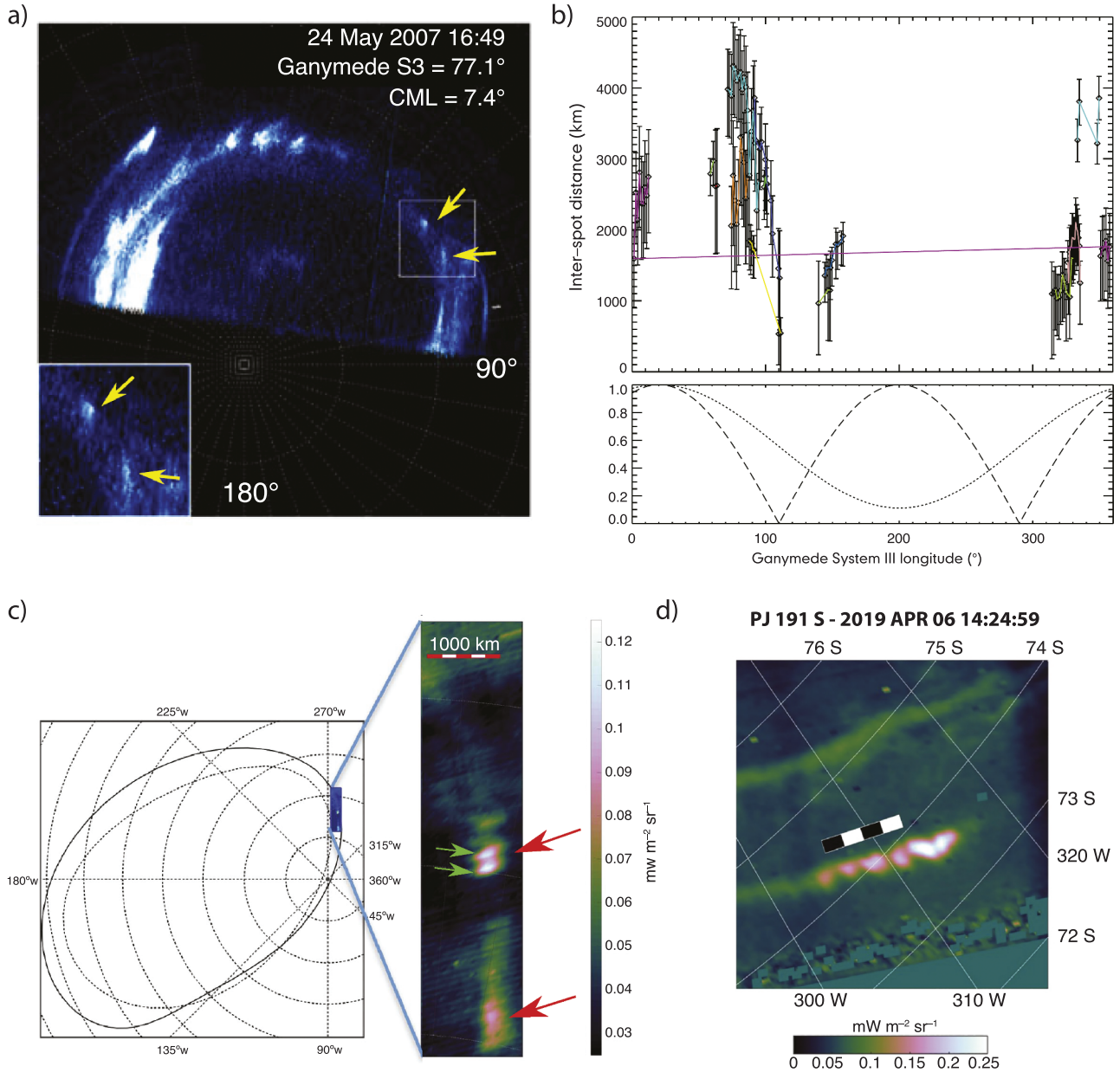

Figure 19.4 (a) Polar projections of an HST UV image acquired on 24 May 2007 at 16:40 UT. Two Ganymede footprint spots can be identified, as highlighted by the arrows. (From Bonfond et al. (2013)). (b) Inter-spot distance between the two spots of the Ganymede footprint. (top) The coloured lines connect points from the same HST orbit. The error bars assume a selection uncertainty of 1 pixel for the first spot and 2 pixels for the second one. (bottom) The long-dashed lines show the expected dependence of the distance for a trans-hemispheric electron beam spot (arbitrary units). In this case, the two spots merged as Ganymede crossed the centrifugal equator. The short-dashed line shows the expected behaviour of the distance for a reflected Alfvén wing (RAW) spot. In this case, the minimum distance is expected when Ganymede is at its northernmost centrifugal latitude (~200° System III longitude). (From Bonfond et al. (2013)). Panels a, b reprinted with permission from John Wiley and Sons. Bonfond, B., Hess, S., Bagenal, F., Gérard, J.-C., Grodent, D., Radioti, A., Gustin, J., and Clarke, J. T. The multiple spots of the Ganymede auroral footprint, *Geophys. Res. Lett.*, 40, 4977–4981 ©2013. (c) Infrared image of the Ganymede footprint spots from the JIRAM instrument on board Juno. We can see that each spot (red arrows) is actually formed from at least two sub-structures (green arrows). (From Mura et al. (2018)). AAPG ©2018. Mura, A., Adriani, A., Connerney, et al. Juno observations of spot structures and a split tail in Io-induced aurorae on Jupiter, *Science* 361(6404), 774–777. Reprinted by permission of the AAPG whose permission is required for further use. (d) Infrared images of the Ganymede footprint tail. The tail is also made of a string of sub-spots. (From Moirano et al. (2021)). Reprinted with permission from John Wiley and Sons. Moirano, A., Mura, A., Adriani, A., Dols, V., Bonfond, B., Waite, J. H., et al. (2021). Morphology of the auroral tail of Io, Europa, and Ganymede from JIRAM L-band imager. *Journal of Geophysical Research: Space Physics*, 126 ©2021.

https://doi.org/10.1017/9781108966474.020 Published online by Cambridge University Press

The Brightness of the Ganymede Footprint

On HST UV images acquired at slant angle, the brightness of the Ganymede footprint can reach up to 180 kR (Wannawichian et al., 2010). The total power emitted by the Ganymede footprint's main spot typically ranges between 1 and 6 GW in the H_2 UV Lyman and Werner bands. However, depending on the auroral background emissions, it can also become so dim that it is no longer identifiable (Bonfond et al., 2017a). The precipitated energy is approximately 10 times higher than the energy of the resulting UV emissions (Gustin et al., 2012). Assuming that 10 per cent of the Poynting flux carried by the Alfvén waves is converted into electron acceleration, this emitted UV power is in the highest part or slightly higher than the range predicted by the models of satellite–magnetosphere interaction (Saur et al., 2013). Because the moon–magnetosphere interaction depends on the local plasma density, the emitted power is the highest when Ganymede is in the center of the plasma sheet and decreases outside of it (Grodent et al., 2009). However, it also varies at two shorter timescales: in the range of 10–40 minutes and in the range of two to three minutes. The first one probably corresponds to Ganymede's traversal time of plasma bubbles with properties differing from the surrounding environment, such as the plasma injections typically observed at such radial distances (Mauk et al., 1997). A detailed analysis of some HST sequences showed the Ganymede footprint disappearing as it traversed the auroral signature of such a plasma injection, further adding confidence into this explanation (Bonfond et al., 2017a). A similar behaviour had already been reported for the Io footprint (Bonfond et al., 2012), and Hess, Bonfond and Delamere (2013) argued that this disappearance was most probably due to the increased electron density at high latitude, which limited the efficiency of the parallel electron acceleration by inertial Alfvén waves. The two- to three-minute timescale could either be related to the recurrence time of bursty magnetic reconnection at the front of Ganymede's magnetosphere, in accordance with the MHD simulations (Jia et al., 2008; Zhou et al., 2019, 2020), or to the quasi-periodic formation, upward migration and disappearance of electric potential drops of a few hundred volts at altitudes around 0.2 R_J above Jupiter's surface. The latter scenario, which is not mutually exclusive with the first one, is proposed in analogy with similar structures found at the Io footprint from observations of fast-drifting radio S-bursts (Hess et al., 2009) and could explain the two- to three-minute fluctuations of the UV brightness of the Io, Europa and Ganymede footprints (Bonfond et al., 2007; Grodent et al., 2009; Bonfond et al., 2017a).

19.3 RADIO EMISSIONS

Induced Radio Emissions

The electrons accelerated in the Alfvén wings to energies of a few keV to tens of keV give rise, close to Jupiter, to intense radio emission via the Cyclotron-Maser Instability (CMI) mechanism (Zarka, 1998; Hess, Mottez and Zarka, 2007; Hess et al., 2008). The emission is produced close to the local electron cyclotron frequency, which can reach 40 MHz in Jupiter's ionosphere (Connerney et al., 2018), and it is beamed at a large angle from the magnetic field in the source (Figures 19.2a,b). The part above 10 MHz (corresponding to the decametre – DAM – wavelength range) can propagate through the Earth's ionosphere and be detected by ground-based antenna arrays, as done by Bigg (1964) and others (e.g. Lamy et al., 2017). Accumulated observations revealed for the Io–Jupiter interaction four islands of enhanced emission occurrence in the Φ_{Io}–CML (Central Meridian Longitude = observer's Jovian System III longitude) plane (Figure 19.3a,b). Those correspond to two physical sources, near both Io Flux Tube (IFT) northern and southern footprints, seen on the eastern and western limbs of the planet because CMI emission is beamed nearly perpendicular to the IFT field lines (Marques et al., 2017) (Figure 19.2b). The high-occurrence islands are not symmetrical around $\Phi_{Io} = 180°$ due to Alfvén wave propagation through Io's torus to Jupiter's ionosphere, which induces a time-variable angular shift (so-called lead angle) that depends on the position of Io in the plasma torus (Figures 19.2c).

Radio Searches

The result from Bigg (1964) demonstrated that existence of a satellite-induced radio emission could be statistically established by building emission occurrence versus the satellite phase Φ, or in the Φ–CML plane. Many observers subsequently searched for the statistical evidence of the interaction of Jupiter's magnetic field with the other Galilean moons plus Amalthea via ground-based DAM observations $\geq$10 MHz, at the Universities of Florida, Chile (narrow-band observations distributed between 15 and 28 MHz), and Colorado (swept-frequency spectrograph 7.6–41 MHz). Lebo et al. (1965) and Bigg (1966) mentioned marginal effects of Europa and Ganymede, but those were not confirmed by subsequent studies involving up to 18 years of accumulated observations (1957–75), that found no other effect than Io's (Dulk, 1967; Kaiser and Alexander, 1973; St. Cyr, 1985). The instruments used had low sensitivity (minimum detectable flux density $\sim 10^4$ Jy = 10^{-22} $Wm^{-2}Hz^{-1}$).

The Galileo plasma wave instrument provided several years of continuous observations (1995–2002) in the hectometre range (2.1–5.6 MHz), that were statistically analyzed in the same way. Low-significance occurrence peaks were found in the $\Phi_{Ganymede}$–CML plane by Menietti et al. (1998a). Including 10 months of Cassini observations, Hospodarsky et al. (2001) found a similar result as well as a marginal dependence on $\Phi_{Callisto}$. Higgins (2007) obtained analog results from the analysis of Voyager 1 and 2 data in the range of 2.1–5.8 MHz. Besides these statistical studies, radio emission induced by Ganymede was tentatively identified through an occultation by Ganymede's body itself (Kurth et al., 1997a) and radio direction-finding by Galileo (Menietti et al., 1998b), and it was proposed as the possible source of rare circular patches observed in Ulysses radio dynamic spectra (Kaiser and MacDowall, 1998). But none of these interpretations was unique and hence convincing.

Radio emissions produced by Ganymede's magnetosphere itself were also discovered at low frequencies ($\leq$100 kHz) by Galileo (Gurnett et al., 1996; Kurth et al., 1997b) (see also Chapter 3.1). These local radio emissions are not generated by the CMI, due to a f_{pe}/f_{ce} ratio > 0.3 close to Ganymede, too high for the CMI to develop, but by conversion of electrostatic waves.

https://doi.org/10.1017/9781108966474.020 Published online by Cambridge University Press

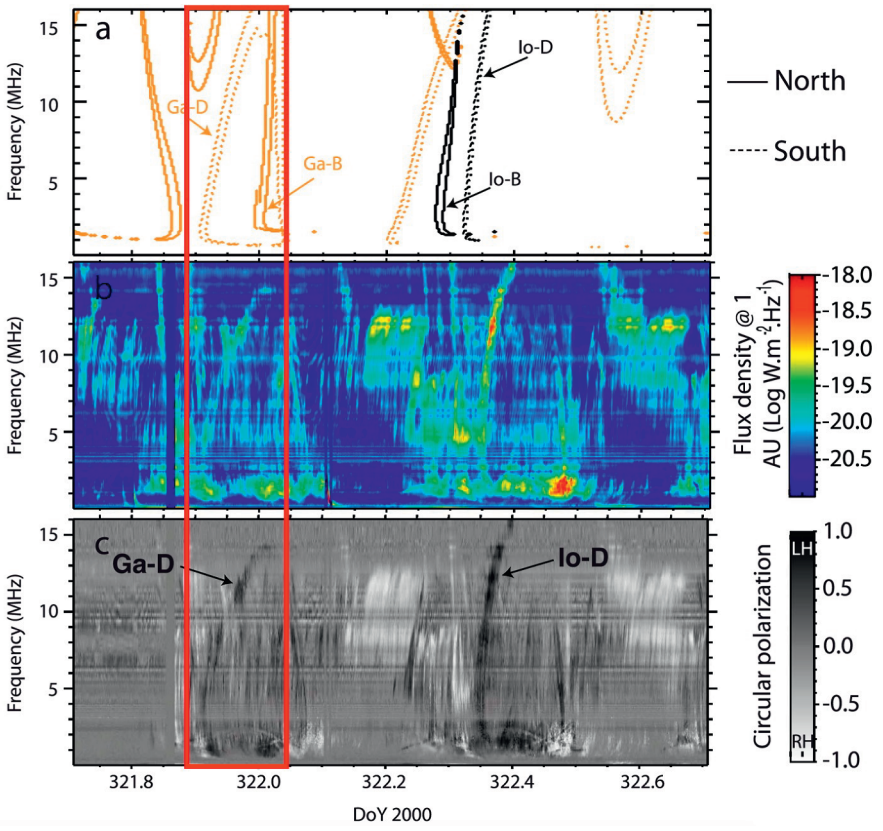

Figure 19.5 (a) ExPRES simulations of Io-induced (in black) and Ganymede-induced (in orange) radio arcs (solid line: northern emissions; dotted line, southern emissions) that should be detected by Cassini during its distant Jupiter flyby of 2000. (b) Dynamic spectrum of flux densities and (c) circular polarization measured by Cassini (LH = left-handed emission from the southern hemisphere; RH = right-handed emission from the northern one). A southern Ganymede D arc is clearly recognized. The background of nested smaller arcs is of auroral origin. From Louis et al. (2017b). Reprinted with permission from John Wiley and Sons. Louis, C. K., Lamy, L., Zarka, P., Cecconi, B., and Hess, S. L., Detection of Jupiter decametric emissions controlled by Europa and Ganymede with Voyager/PRA and Cassini/RPWS, *J. Geophys. Res. Space Physics*, 122, 9228–9247 ©2017.

Radio Detections

Three recent studies detected independently and unambiguously the DAM emissions induced by Ganymede in Jupiter's magnetic field.

Louis et al. (2017a) was based on simulations by the ExPRES code (published in (Louis et al., 2019)). This code, based on CMI physics, predicts the shape of radio arcs in the time-frequency plane for a selected observer's position or trajectory relative to Jupiter. For satellite–Jupiter interactions, that results in an 'active' magnetic flux tube (where electron acceleration takes place – Figure 19.2c) and thus a radio source of limited size; the predicted arcs are well defined and locally isolated in the time-frequency plane rather than being drowned in a series of nested arcs as is the case for auroral DAM (Figure 19.5). ExPRES simulations were compared to Voyager and Cassini radio observations in (Louis et al., 2017a,b), leading to the identification of ∼100 Ganymede–Jupiter radio arcs around $\Phi_{Ganymede} \sim 100°$ and 260°, in broad CML ranges. These ranges of $\Phi_{Ganymede}$ and CML correspond to Ganymede's Jovian longitude of $\Lambda_{Ganymede} = 160°$–$300°$ in the northern hemisphere and $\Lambda_{Ganymede} = 0°$–$100°$ in the southern hemisphere ($\Lambda_{Ganymede} = CML + 180° - \Phi_{Ganymede}$). Radio arcs cover the spectral ranges ∼1–30 MHz in the north and ∼1–16 MHz in the south. Their duration is ∼40–60 minutes. The typical energy of the electrons in ExPRES simulations matching the observations is a few keV.

Zarka et al. (2018) performed a statistical study similar to those of the earlier radio searches described previously, but this time applied to a much longer database, consisting of 26 years of daily observations of Jupiter with the Nançay Decameter Array in the range of 10–40 MHz, with a sensitivity $\sim 1.5 \times 10^3$ Jy, that is, ∼7 times better than earlier observations (Marques et al., 2017). With this database, islands of enhanced occurrence clearly showed up in the $\Phi_{Ganymede}$–CML plane (Figures 19.3d,e), with a signal-to-noise ratio of up to 13σ. These islands, strongly reminiscent of Io–Jupiter ones, cover the ranges of Ganymede phases $65° \pm 40°$ and $225° \pm 35°$ at CML around 155° and 310° respectively, and gather 360 Ganymede–Jupiter emissions. They correspond to a range of Ganymede's longitude $220° \pm 50°$ (Figure 19.3f), very similar to the range of Io's longitudes for which Io-DAM emission is detected (Figure 19.3c). Northern emissions reach 33 MHz and southern ones 27 MHz. The difference in the CML and $\Phi_{Ganymede}$ ranges found by Louis et al. (2017a) can be explained by the different spectral ranges covered by the observations and by the slightly different Jovian latitudes of the observers. The fact that Ganymede–Jupiter emissions do not reach frequencies as

https://doi.org/10.1017/9781108966474.020 Published online by Cambridge University Press

high as the Io–Jupiter ones (~40 MHz) is due to the fact that the northern footprint of the Ganymede flux tube (latitude ~75°) lies northward of the northern high-amplitude magnetic anomaly at the surface of Jupiter crossed by the northern Io flux tube footprint (latitude ~66°), implying that lower electron cyclotron frequencies are reached at Ganymede's flux tube footprint.

The third study is the in situ exploration by Juno of Ganymede's wake, described in the next section.

19.4 IN SITU OBSERVATIONS ASSOCIATED WITH THE GANYMEDE FOOTPRINT

Juno's orbit and instrument suite are particularly well suited to combine remote-sensing observations of the auroral emissions and in situ measurements of the particles and waves giving rise to these emissions. In particular, on 29 May 2019, during Juno's 20th perijove operations, between 07:37:14 and 07:37:32, the spacecraft crossed Ganymede's footpath (i.e. the mapping of Ganymede's orbit along the magnetic field lines) only 8° downstream of the footprint's main spot, as observed from the Juno UltraViolet Spectrograph (Juno-UVS). All in situ instruments showed clear signatures of the crossing (Szalay et al., 2020a). For example, the magnetometer data recorded evidence of both significant field-aligned currents (in the form of deviations of the azimuthal magnetic field component δB_ϕ) and strong Alfvénic activity with Poynting fluxes ~100 mW/m^2 (see Figure 19.6(2d)). On the other hand, the JADE (Jovian Auroral Distributions Experiment) particle instrument recorded field-aligned enhancement of the electron flux in both directions (see Figure 19.6(2a), (2b) and (2c)). The precipitating electrons' energy flux reached 11 mW/m^2, which is ~10 per cent of the Poynting energy flux. The electron energy distribution did not show a peaked feature, which would be expected from acceleration by a discrete quasi-static electric field, but a broadband enhancement in the range from 0.5 to 40 keV, compatible with an Alfvénic acceleration process.

From the crossing time, the inferred width of the whole footprint tail is 660 km; however, the current system is highly structured, and smaller-scale (~50 km) sub-structures also are apparent in the JADE data. Moreover, the pitch angle distribution shows that the electron acceleration is bi-directional since a significant flux of upwards-moving electrons was observed. Finally, JADE measurements also revealed upward electron conics in downward currents, which further bolsters the explanation involving particle acceleration by inertial Alfvén waves near the Jovian ionosphere. These findings, as well as the discovery of a similar accelerated broadband electron distribution in the Europa footprint tail (Allegrini et al., 2020), further strengthen the idea that similar processes are at play for all footprints.

During the same event, Juno also crossed the source region of the decametric radio emissions related to the Ganymede footprint tail (Louis et al., 2020, Figure 19.6 1). Measurements by Juno/Waves and JADE showed that these decametric emissions are produced slightly (0.5–2.1%) above the local f_{ce} and beamed at 76° to 83° from the magnetic field. These results are fully consistent with their generation by the loss-cone-driven CMI (as opposed to a shell-driven one that would generate perpendicular waves). The electrons triggering these emissions, likely accelerated by Alfvén waves, have an energy of 4–15 keV. The size of the radio source region was at least 250±50 km wide perpendicular to the magnetic field. It is spread along thousands of kilometres along the field lines, different frequencies being emitted at different altitudes, where $f \sim f_{ce}$; as a rule of thumb, 1 kHz bandwidth corresponds to ~1 km extent along Jovian high-latitude field lines.

19.5 WHAT ELECTROMAGNETIC EMISSIONS FROM SATELLITE FOOTPRINTS TEACH US ON MAGNETOSPHERIC PHYSICS

The Ganymede Footprint as a Landmark in the Jovian Magnetosphere

The satellite footprints are extremely valuable landmarks in the aurora, as they directly connect via magnetic field lines the associated moons at their orbital distance to their ionospheric conjugates. The location of the Io footprint has thus been used as a constraint to increase the accuracy of the internal magnetic field models. For example, the VIP4 (Voyager, Io, Pioneer, 4th order) magnetic field model uses infrared observations of the Io footpath location to complement the in situ magnetic measurements from the Pioneer and Voyager spacecraft and increase the model accuracy in the polar regions (Connerney et al., 1998). However, an analysis of the footpaths of Io, Europa and Ganymede based on HST UV observations in the northern hemisphere showed that the three contours diverge in the region centered around 100° System III longitude (Grodent et al., 2008). The peculiar shape of the different footpaths could be reproduced by adding a small localized dipole magnetic field to the global multipolar magnetic field model, interpreted as indicative of a localized magnetic anomaly. The VIPAL (Voyager, Io, Pioneer, Anomaly, Longitudes) model was based on a larger set of UV observations, using both the latitude and the longitude of the Io footprint's main spot (rather than just the footpath location) to improve the model's accuracy, especially in the magnetic anomaly region (Hess and Delamere, 2012). Finally, the ISaAC (In Situ and Auroral Constrains) model (Hess et al., 2017) used the same technique, but also accounting for the location of the Europa and Ganymede footprints to further refine the model. In the polar regions, the result was indeed remarkably close to the later results from the JRM09 model, which is derived solely from the highly accurate magnetic field measurements from Juno's first nine orbits (Connerney et al., 2018). Juno's measurements also confirmed the presence and location of the magnetic anomaly in the northern polar region. It should be noted, however, that only Juno's measurements could identify the larger magnetic anomaly often named the 'Big Blue Spot', which is located much closer to the equator (Moore et al., 2017; Connerney et al., 2018), where footprint locations provide no useful constraints.

The size of the contour of the main auroral emissions at Jupiter can change from one Jovian rotation to another, superimposed onto long-term trends over a few months (Bonfond et al., 2012). It is, however, challenging to infer whether these changes are related to variations of the radial distance from which these auroras originate, or to the variable stretching of

https://doi.org/10.1017/9781108966474.020 Published online by Cambridge University Press

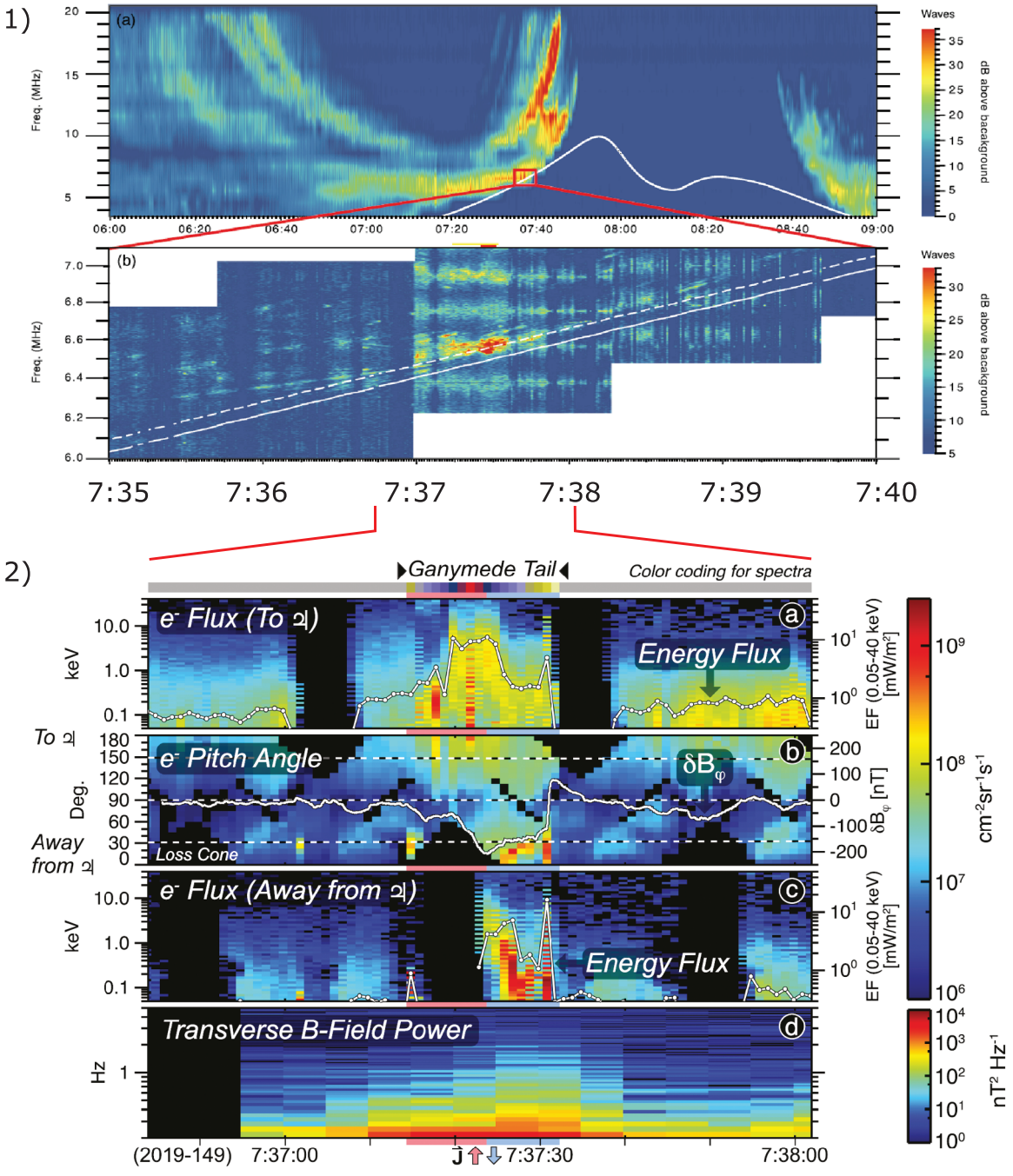

Figure 19.6 JADE, MAG and WAVES data during the Ganymede footprint tail flux tube encounter of 2019. (1a) Low-resolution Juno/Waves data and (1b) zoom at high resolution. The solid white line is the electron cyclotron frequency f_{ce} measured by Juno's magnetometer, and the dashed white line is $1.01 \times f_{ce}$ (adapted from Louis et al. (2020)). Reprinted with permission from John Wiley and Sons. Louis, C. K., Louarn, P., Allegrini, F., Kurth, W. S., & Szalay, J. R. Ganymede-induced decametric radio emission: In situ observations and measurements by Juno. *Geophysical Research Letters*, 47, ©2020. Panels (2a) and (2c) show the downward and upward electron differential energy flux (DEF) within the loss cone, respectively. Precipitating energy flux is overlaid on these panels with its separate axes on the right of the spectrograms. Panel (2b) shows electron pitch angles with δB_ϕ overlaid. Panel (2d) shows the transverse B field power spectral densities. Red/blue bars indicate approximate upward/downward current regions inferred from MAG data. (From Szalay et al. (2020a)). Reprinted with permission from John Wiley and Sons. Szalay, J. R., Allegrini, F., Bagenal, F., Bolton, S. J., Bonfond, B., Clark, G., et al. (2020). Alfvénic acceleration sustains Ganymede's footprint tail aurora. *Geophysical Research Letters*, 47, ©2020.

the magnetic field lines. At Ganymede's distance from Jupiter, the influence on the mapping of the current sheet's magnetic field, which distorts the magnetic field radially, is much larger than at Io's. Grodent et al. (2008b) indeed noted that, while the location of the Io footpath remained remarkably stable through time, the magnetic latitude of the Ganymede footpath could move by as much as 2.4° and the main emissions by ~3°. Such a shift could be reproduced by modifying the current sheet thickness from $5R_J$ to $2.5R_J$ in the VIP4 model (Connerney et al., 1998), which uses the current sheet model of Connerney (1981). Moreover, on at least one occasion, the Ganymede footprint was seen inside the main emissions instead of outside

https://doi.org/10.1017/9781108966474.020 Published online by Cambridge University Press

(Bonfond et al., 2012). Not only did the main emissions expand equatorward down to Ganymede, but the Ganymede footprint itself had moved out by 0.5°. This unique observation indicated that both the stretching of the magnetic field lines and the radial distance of the region mapping to the main emissions can change through time.

Finally, magnetic field models based on multi-polar developments of the internal field and an axisymmetric representation of the current sheet, such as VIP4, VIPAL, ISaAC or JRM09, are increasingly inaccurate beyond 30 R_J. In particular, local time effects become increasingly important beyond this distance (Khurana, 1997). An alternative method to field tracing models is based on the flux equivalence principle (Vogt et al., 2011, 2015). Starting from a distance where the mapping is known, the iterative construction of this mapping model consists of finding the ionospheric counterpart of an elemental area in the equatorial magnetosphere by equating the magnetic flux in the two regions. Again, the footpath of Ganymede serves as a reliable reference point, from which contours at increasingly large distances in the magnetosphere are progressively mapped into the ionosphere.

Radio Emissions Durations

The duration of Io–Jupiter DAM emissions was found to be statistically twice that of auroral DAM emissions (Marques et al., 2017; Zarka et al., 2018). This can be understood because auroral DAM is controlled by Jupiter's rotation of period ∼10 h whereas Io–Jupiter DAM is primarily controlled by Io's orbital motion of period ∼42 h, combined with a narrow radio beaming and a steady Alfvén wings system fixed (at first order) relative to Io. Ganymede's orbital period being four times that of Io, one might have expected, in the case of steady magnetic reconnection and Alfvén wings attached to that moon, a duration of Ganymede–Jupiter DAM emissions statistically longer than for Io. Zarka et al. (2018) developed a method for comparing the broad distributions of durations of these radio emissions, and not only their moments. They showed that the duration of Ganymede–induced DAM radio bursts, between ∼10 min. and ∼3 h 30, was statistically 1.7 times shorter than that of Io–Jupiter ones, and only ∼1.2 times longer than auroral DAM bursts. This implies that Ganymede–Jupiter interaction is dominated by Jupiter's rotation.

One possible explanation is that the efficiency of the reconnection between Jupiter and Ganymede magnetic fields varies with Jupiter's rotation. Analyzing an analytical criterion for reconnection onset, Kaweeyanun et al. (2020) found that reconnection may occur anywhere on Ganymede's magnetopause in an unpredictable, disordered way, the average reconnection rate being controlled by the ambient Jovian field orientation and hence driven by Jupiter's rotation. Magnetohydrodynamics simulations (Jia et al., 2009, 2010) and MHD-Hall simulations (Zhou et al., 2019, 2020) also showed that magnetic reconnection is intrinsically intermittent, involving flux ropes and flux transfer events at timescales down to 10–100 s near the upstream magnetopause, even for constant external conditions. But these timescales are much shorter than the duration of Ganymede–induced DAM radio bursts.

Another explanation is that the conditions permitting CMI emission at Ganymede's footprints (for example, the magnetic field topology favouring the existence of a loss cone) exist in a range of longitudes more restricted than those for Io. This is indeed what is suggested by Figures 19.3c and 19.3f. Combined with the synodic period of Jupiter relative to Ganymede being shorter than the synodic period of Jupiter relative to Io, this explains the statistically shorter durations of Ganymede-induced radio bursts.

This, and the persistence of the UV footprints of Ganymede, suggests that the remote electrodynamic interaction between Ganymede and the Jovian magnetic field is rather steady, and consequently that the electrons responsible for the electromagnetic footprint emissions are likely accelerated by Alfvén waves rather than by reconnection.

Radio Emissions Energetics

Kurth et al. (2000) qualitatively compared the strength of the local and distant radio emissions and plasma waves at the four Galilean moons, noting that it is strongest at Io and 'intermediate' at Europa and Ganymede. Zarka (2007) extended this comparison to the power emitted in UV footprints and induced CMI radio emissions, still poorly constrained at that time. Grodent et al. (2009) better quantified the power emitted in the UV by Ganymede's footprint (0.2–1.5 GW). Following their statistical detection of Ganymede-induced radio emissions, Zarka et al. (2018) measured their intensity (marginally lower than Io-induced ones) and their emitted power (∼15× lower than for Io-induced radio emissions). This strengthened the radio-magnetic scaling law proposed in (Zarka et al., 2001; Zarka, 2007) and generalized in figure 7 of (Zarka et al., 2018) that relates the emitted radio power to the intercepted Poynting flux (or magnetic energy flux) in all interactions involving a magnetized plasma flow (sub- or super-Alfvénic) and an obstacle (magnetized or not). According to this scaling law, the dissipated electromagnetic power writes in all cases

$$P_{dissipated}(W) \simeq \epsilon(V_{flow}B^2_{\perp flow}/\mu_o)\pi R^2_{obstacle}, \tag{19.1}$$

with $B_{\perp flow}$ the flow's magnetic field component perpendicular to the flow direction in the obstacle's frame, and an efficiency $0 < \epsilon \leq 1$ ($\epsilon \simeq M_A$, the Alfvén Mach number, for a sub-Alfvénic flow). Following Equation (19.1), the dissipated power (from the intercepted Jovian magnetic field) in the Alfvén wings is similar for Europa and Ganymede, Europa being closer to Jupiter but Ganymede having a much larger cross section due to its magnetosphere, and about one order of magnitude smaller than in Io's Alfvén wings. Furthermore, it was found in (Zarka et al., 2001; Zarka, 2007) that the emitted radio power resulting from the flow–obstacle interaction follows the relation

$$P_{radio}(W) \simeq \beta(V_{flow}B^2_{\perp flow}/\mu_o)\pi R^2_{obstacle} = (\beta/\epsilon)P_{dissipated}, \tag{19.2}$$

with an efficiency factor $\beta = 2 - 10 \times 10^{-3}$. Subsequent works explored the theoretical foundations of this radio-magnetic scaling law and found that it only provides order-of-magnitude estimates (see (Zarka, 2020) and references therein), but as it seems to hold over >10 orders of magnitude, it remains adapted to predictions and analyses of populations. In particular, the Ganymede–Jupiter interaction provides a useful model for studying star–planet plasma interactions in which a magnetized hot Jupiter interacts with its magnetized parent star, and also possibly some pulsar–planet interactions.

https://doi.org/10.1017/9781108966474.020 Published online by Cambridge University Press

19.6 SUMMARY AND PERSPECTIVES

Summary

Thanks to the data collected by Galileo during its six close flybys of Ganymede in 1995–2000, and by HST, Juno and ground-based radio telescopes, the electrodynamic coupling between Ganymede and the Jovian ionosphere thus seems to be fairly well described and understood at first order. Despite the very different nature of the local interaction close to the satellites, the processes taking place further away from them appear common to all moons, suggesting that there is a universal physics at play, applicable to other systems as well, even beyond our solar system. Among these processes are the prominent role of Alfvén waves, not only to carry the electric current but also to accelerate the electrons along the field lines in both directions. Another common characteristic is the presence of short length-scale features and short timescale variations of the footprints, even if the characteristics of these behaviours are not yet fully elucidated. Moreover, the characteristics of the radio decametric emissions at both Io and Ganymede demonstrate the importance of the cyclotron-maser instability, and the power of the decametric emissions at Ganymede helped validate the scaling law between the emitted radio power and the intercepted Poynting flux. Finally, the location of the Ganymede auroral footprint has also served as a useful landmark to both constrain the internal magnetic field models before the arrival of Juno and to map auroral features into the magnetosphere.

Open Questions and Perspectives

In addition to its use as a reference point in the magnetosphere, a careful analysis of the magnetic footprint of Ganymede could even help us to get one step further: documenting the changes in the Jovian magnetosphere. The footprint could be a tool to monitor the state of the magnetosphere, by studying both the latitudinal position of the spots and their spacing. The first one is related to the azimuthal currents in the plasma sheet, while the second varies directly with the Alfvén propagation time, which depends on the plasma density and the magnetic field strength. However, to achieve such an objective, a calibration of the relationship between auroral and magnetospheric parameters remains to be performed.

The coordinates of the high-occurrence islands in the $\Phi_{Ganymede}$–CML plane (Figures 19.3d,e), as well as their extension to nearly all CML and different Ganymede phases at low frequencies (Louis et al., 2017b), remain to be quantitatively explained. Another open question concerning radio emissions is the existence of Ganymede-induced S-bursts and the spatial structure of electric fields and electrons' acceleration along the Ganymede flux tube (e.g., (Hess, Zarka and Mottez, 2007; Hess et al., 2009) for Io).

It would be interesting to search in radio and UV data for direct signatures of the intermittent reconnection between Jupiter's and Ganymede's magnetic fields, and more broadly to correlate the occurrence of radio and UV emissions at all timescales. However, this quest will not be simple, because short-timescale (a few minutes) variations of the footprint brightness, which could result from those bursty reconnections, have also been identified at Io and Europa, where reconnection is not expected (Bonfond et al., 2017a).

These two processes are not mutually exclusive and will thus be difficult to disentangle. Furthermore, the sub-structure of the Ganymede footprint spots could also be interpreted as a signature of the reconnection sites at the front and back of Ganymede's magnetosphere (Mura et al., 2018). However, here again, a similar spatial pattern has been identified at Io's footprint, which also calls for a common explanation.

Many pieces of the scenario proposed to explain the footprint spots' multiplicity, such as the measurements of strong Alfvén waves and bi-directional electron beams with a broad energy distribution, have been confirmed by in situ measurements. However, a clear demonstration that the electrons accelerated away from Jupiter in one hemisphere can actually precipitate in the opposite one remains to be found.

Finally, one of the most unexpected findings of Juno regarding the satellite footprints was the discovery of proton beams during Io's Alfvén wings crossings, with three different acceleration regions identified, at altitudes between 0.9 and 2.5 R_J at the torus boundary and very close to Jupiter at altitudes around 0.16 R_J (Szalay et al., 2020b; Clark et al., 2020). The two former populations probably arise from Alfvénic acceleration, while the third possibly stems from interactions with ion-cyclotron waves (Sulaiman et al., 2020). The first indications that a similar process also takes place at Ganymede need to be confirmed (Szalay et al., 2020a). Similarly, energetic proton depletion found in Io's wake (Paranicas et al., 2019) probably has a counterpart at Ganymede, even if it hasn't been found yet.

While the Juno mission is essentially dedicated to Jupiter itself, the European JUpiter ICy moons Explorer (JUICE) mission, which was launched on 14 April 2023, will further investigate Ganymede and its surrounding space environment (Grasset et al., 2013). After a first phase of the mission orbiting around Jupiter and flying by Europa, Ganymede and Callisto, the spacecraft is planned to insert into Ganymede's orbit. This mission profile will allow it to connect directly for the first time in situ measurements of particles and fields near Ganymede (e.g. signatures of reconnection), or observations of the incoming Jovian magnetospheric plasma via energetic neutral atoms (ENAs) imaging, to simultaneous multi-wavelength remote-sensing observations of Ganymede's auroral footprint on Jupiter. Such observations will be instrumental to discriminate the many processes involved in the electrodynamic interaction and answer the questions listed earlier.

REFERENCES

Allegrini, F., Gladstone, G. R., Hue, V. et al. (2020), 'First report of electron measurements during a Europa footprint tail crossing by Juno', *Geophysical Research Letters* **47**(18), e2020GL089732. eprint: https://agupubs.onlinelibrary.wiley.com/doi/pdf/10.1029/2020GL089732. **URL:** https://agupubs.onlinelibrary.wiley.com/doi/abs/10.1029/2020GL089732.

Badman, S. V., Branduardi-Raymont, G., Galand, M. et al. (2015), 'Auroral processes at the giant planets: energy deposition, emission mechanisms, morphology and spectra', *Space Science Reviews* **187**(1), 99–179. **URL:** https://doi.org/10.1007/s11214-014-0042-x.

Bhattacharyya, D., Clarke, J. T., Montgomery, J. et al. (2018), 'Evidence for auroral emissions from Callisto's footprint in HST UV images', *Journal of Geophysical Research: Space Physics* **123**(1),

https://doi.org/10.1017/9781108966474.020 Published online by Cambridge University Press

364–73. **URL:** https://agupubs.onlinelibrary.wiley.com/doi/abs/10.1002/2017JA024791.

Bigg, E. K. (1964), 'Influence of the Satellite Io on Jupiter's decametric emission', *Nature* **203**(4949), 1008–10. **URL:** www.nature.com/articles/2031008a0.

Bigg, E. K. (1966), 'Periodicities in Jupiter's decametric radiation', *Planetary and Space Science* **14**(8), 741–58.

Bonfond, B., Gérard, J.-C., Grodent, D. and Saur, J. (2007), 'Ultraviolet Io footprint short timescale dynamics', *Geophysical Research Letters* **34**, L06201, doi:https://doi.org/10.1029/2006GL028765. **URL:** https://agupubs.onlinelibrary.wiley.com/doi/abs/10.1029/2006GL028765.

Bonfond, B., Grodent, D., Badman, S. V. et al. (2017a), 'Similarity of the Jovian satellite footprints: spots multiplicity and dynamics', *Icarus* **292**, 208–17. **URL:** www.sciencedirect.com/science/article/pii/S0019103516304547.

Bonfond, B., Grodent, D., Gérard, J.-C. et al. (2009), 'The Io UV footprint: location, inter-spot distances and tail vertical extent', *Journal of Geophysical Research: Space Physics* **114**, A07224, doi:https://doi.org/10.1029/2009JA014312. **URL:** https://agupubs.onlinelibrary.wiley.com/doi/abs/10.1029/2009JA014312.

Bonfond, B., Grodent, D., Gérard, J.-C. et al. (2012), 'Auroral evidence of Io's control over the magnetosphere of Jupiter', *Geophysical Research Letters* **39**, L01105, doi:https://doi.org/10.1029/2011GL050253. **URL:** https://agupubs.onlinelibrary.wiley.com/doi/abs/10.1029/2011GL050253.

Bonfond, B., Hess, S., Bagenal, F. et al. (2013), 'The multiple spots of the Ganymede auroral footprint', *Geophysical Research Letters* **40**(19), 4977–81. **URL:** https://agupubs.onlinelibrary.wiley.com/doi/abs/10.1002/grl.50989.

Bonfond, B., Saur, J., Grodent, D. et al. (2017), 'The tails of the satellite auroral footprints at Jupiter', *Journal of Geophysical Research: Space Physics* **122**(8), 7985–96. **URL:** https://agupubs.onlinelibrary.wiley.com/doi/abs/10.1002/2017JA024370.

Chust, T., Roux, A., Kurth, W. S. et al. (2005), 'Are Io's Alfvén wings filamented? Galileo observations', *Planetary and Space Science* **53**(4), 395–412. **URL:** www.sciencedirect.com/science/article/pii/S003206330400159X.

Clark, G., Mauk, B. H., Kollmann, P. et al. (2020), 'Energetic proton acceleration associated with Io's footprint tail', *Geophysical Research Letters* **47**(24), e2020GL090839. eprint: https://agupubs.onlinelibrary.wiley.com/doi/pdf/10.1029/2020GL090839. **URL:** https://onlinelibrary.wiley.com/doi/abs/10.1029/2020GL090839.

Clarke, J. T., Ajello, J., Ballester, G. et al. (2002), 'Ultraviolet emissions from the magnetic footprints of Io, Ganymede and Europa on Jupiter', *Nature* **415**(6875), 997–1000. **URL:** www.nature.com/articles/415997a.

Collinson, G., Paterson, W. R., Bard, C. et al. (2018), 'New results from Galileo's first flyby of Ganymede: reconnection-driven flows at the low-latitude magnetopause boundary, crossing the cusp, and icy ionospheric escape', *Geophysical Research Letters* **45**(8), 3382–92. eprint: https://agupubs.onlinelibrary.wiley.com/doi/pdf/10.1002/2017GL075487. **URL:** https://agupubs.onlinelibrary.wiley.com/doi/abs/10.1002/2017GL075487.

Connerney, J. E. P. (1981), 'The magnetic field of Jupiter: a generalized inverse approach', *Journal of Geophysical Research: Space Physics* **86**(A9), 7679–93. **URL:** https://agupubs.onlinelibrary.wiley.com/doi/abs/10.1029/JA086iA09p07679.

Connerney, J. E. P., Acuña, M. H., Ness, N. F. and Satoh, T. (1998), 'New models of Jupiter's magnetic field constrained by the Io flux tube footprint', *Journal of Geophysical Research: Space Physics* **103**(A6), 11929–9. **URL:** https://agupubs.onlinelibrary.wiley.com/doi/abs/10.1029/97JA03726.

Connerney, J. E. P., Baron, R., Satoh, T. and Owen, T. (1993), 'Images of excited $H3^+$ at the foot of the lo flux tube in Jupiter's atmosphere', *Science* **262**(5136), 1035–38. **URL:** https://science.sciencemag.org/content/262/5136/1035.

Connerney, J. E. P., Kotsiaros, S., Oliversen, R. J., Espley, J. R. et al. (2018), 'A new model of Jupiter's magnetic field from Juno's first nine orbits', *Geophysical Research Letters* **45**(6), 2590–6. **URL:** https://agupubs.onlinelibrary.wiley.com/doi/abs/10.1002/2018GL077312.

Damiano, P. A., Delamere, P. A., Stauffer, B., Ng, C.-S. and Johnson, J. R. (2019), 'Kinetic simulations of electron acceleration by dispersive scale Alfvén waves in Jupiter's magnetosphere', *Geophysical Research Letters* **46**(6), 3043–51. eprint: https://agupubs.onlinelibrary.wiley.com/doi/pdf/10.1029/2018GL081219. **URL:** https://agupubs.onlinelibrary.wiley.com/doi/abs/10.1029/2018GL081219.

Delamere, P. A., Bagenal, F., Ergun, R. and Su, Y.-J. (2003), 'Momentum transfer between the Io plasma wake and Jupiter's ionosphere', *Journal of Geophysical Research: Space Physics* **108**(A6). **URL:** https://agupubs.onlinelibrary.wiley.com/doi/abs/10.1029/2002JA009530.

Dulk, G. A. (1967), 'Lack of effects of satellites Europa, Ganymede, Callisto, and Amalthea on the decametric radio emission of Jupiter', *The Astrophysical Journal* **148**, 239.

Ergun, R. E., Su, Y.-J., Andersson, L. et al. (2006), 'S bursts and the Jupiter ionospheric Alfvén resonator', *Journal of Geophysical Research: Space Physics* **111**, A06212, doi: https://doi.org/10.1029/2005JA011253. **URL:** https://agupubs.onlinelibrary.wiley.com/doi/abs/10.1029/2005JA011253.

Goldreich, P. and Lynden-Bell, D. (1969), 'Io, a Jovian unipolar inductor', *The Astrophysical Journal* **156**, 59–78.

Grasset, O., Dougherty, M. K., Coustenis, A. et al. (2013), 'JUpiter ICy moons Explorer (JUICE): an ESA mission to orbit Ganymede and to characterise the Jupiter system', *Planetary and Space Science* **78**, 1–21. **URL:** www.sciencedirect.com/science/article/pii/S0032063312003777.

Grodent, D., Bonfond, B., Gérard, J.-C. et al. (2008), 'Auroral evidence of a localized magnetic anomaly in Jupiter's northern hemisphere', *Journal of Geophysical Research: Space Physics* **113**, A09201, doi:https://doi.org/10.1029/2008JA013185. **URL:** https://agupubs.onlinelibrary.wiley.com/doi/abs/10.1029/2008JA013185.

Grodent, D., Bonfond, B., Radioti, A. et al. (2009), 'Auroral footprint of Ganymede', *Journal of Geophysical Research: Space Physics* **114**, A07212, doi:https://doi.org/10.1029/2009JA014289. https://agupubs.onlinelibrary.wiley.com/doi/abs/10.1029/2009JA014289.

Grodent, D., Gérard, J.-C., Radioti, A., Bonfond, B. and Saglam, A. (2008b), 'Jupiter's changing auroral location', *Journal of Geophysical Research: Space Physics* **113**, A01206, doi:https://doi.org/10.1029/2007JA012601. eprint: https://agupubs.onlinelibrary.wiley.com/doi/pdf/10.1029/2007JA012601. **URL:** https://agupubs.onlinelibrary.wiley.com/doi/abs/10.1029/2007JA012601.

Gurnett, D. A. and Goertz, C. K. (1981), 'Multiple Alfven wave reflections excited by Io: Origin of the Jovian decametric arcs', *Journal of Geophysical Research* **86**(A2), 717–22.

Gurnett, D. A., Kurth, W. S., Roux, A., Bolton, S. J. and Kennel, C. F. (1996), 'Evidence for a magnetosphere at Ganymede from plasma-wave observations by the Galileo spacecraft', *Nature* **384**(6609), 535–7. **URL:** www.nature.com/articles/384535a0.

Gustin, J., Bonfond, B., Grodent, D. and Gérard, J.-C. (2012), 'Conversion from HST ACS and STIS auroral counts into brightness, precipitated power, and radiated power for H2 giant planets', *Journal of Geophysical Research: Space Physics* **117**, A07316, doi:https://doi.org/10.1029/2012JA017607. **URL:** https://agupubs.onlinelibrary.wiley.com/doi/abs/10.1029/2012JA017607.

Hess, S., Bonfond, B., Bagenal, F. and Lamy, L. (2017), *A Model of the Jovian Internal Field Derived from In-Situ and Auroral Constraints*. Austrian Academy of Sciences Press. **URL:** https://orbi.uliege.be/handle/2268/221222.

Hess, S. and Delamere, P. (2012), Satellite-Induced Electron Acceleration and Related Auroras, in A. Keiling, E. Donovan, F. Bagenal and T. Karlsson, eds., *Auroral Phenomenology and Magnetospheric Processes: Earth and Other Planets*, American Geophysical Union. **URL:** http://onlinelibrary.wiley.com/doi/10.1029/2011GM001175/summary.

Hess, S. L. G., Bonfond, B., Chantry, V. et al. (2013), 'Evolution of the Io footprint brightness II: modeling', *Planetary and Space Science* **88**, 76–85. **URL:** www.sciencedirect.com/science/article/pii/S0032063313002109.

Hess, S. L. G., Bonfond, B. and Delamere, P. A. (2013), 'How could the Io footprint disappear?', *Planetary and Space Science* **89**, 102–10. **URL:** www.sciencedirect.com/science/article/pii/S0032063313002195.

Hess, S. L. G., Delamere, P., Dols, V., Bonfond, B. and Swift, D. (2010), 'Power transmission and particle acceleration along the Io flux tube', *Journal of Geophysical Research: Space Physics* **115**, A06205, doi:https://doi.org/10.1029/2009JA014928. https://agupubs.onlinelibrary.wiley.com/doi/abs/10.1029/2009JA014928.

Hess, S., Mottez, F. and Zarka, P. (2007), 'Jovian S burst generation by Alfvén waves', *Journal of Geophysical Research: Space Physics* **112**(A11), A11212.

Hess, S., Mottez, F., Zarka, P. and Chust, T. (2008), 'Generation of the Jovian radio decametric arcs from the Io flux tube', *Journal of Geophysical Research: Space Physics* **113**(A3), A03209.

Hess, S., Zarka, P. and Mottez, F. (2007), 'Io Jupiter interaction, millisecond bursts and field-aligned potentials', *Planetary and Space Science* **55**(1–2), 89–99.

Hess, S., Zarka, P., Mottez, F. and Ryabov, V. B. (2009), 'Electric potential jumps in the Io-Jupiter flux tube', *Planetary and Space Science* **57**(1), 23–33. **URL:** www.sciencedirect.com/science/article/pii/S0032063308003358.

Higgins, C. A. (2007), 'Satellite control of Jovian 2–6 MHz radio emission using Voyager data', *Journal of Geophysical Research: Space Physics* **112**, A05213, doi:https://doi.otg/10.1029/2006JA012100. eprint: https://agupubs.onlinelibrary.wiley.com/doi/pdf/10.1029/2006JA012100. **URL:** https://agupubs.onlinelibrary.wiley.com/doi/abs/10.1029/2006JA012100.

Hill, T. W. and Vasyliunas, V. M. (2002), 'Jovian auroral signature of Io's corotational wake', *Journal of Geophysical Research* **107**(A12), 1464.

Hinson, D. P., Kliore, A. J., Flasar, F. M. et al. (1998), 'Galileo radio occultation measurements of Io's ionosphere and plasma wake', *Journal of Geophysical Research* **103**(A12), 29343–58.

Hinton, P. C., Bagenal, F. and Bonfond, B. (2019), 'Alfvén wave propagation in the Io plasma torus', *Geophysical Research Letters* **46**(3), 1242–9. eprint: https://agupubs.onlinelibrary.wiley.com/doi/pdf/10.1029/2018GL081472. **URL:** https://agupubs.onlinelibrary.wiley.com/doi/abs/10.1029/2018GL081472.

Hospodarsky, G. B., Christopher, I. W., Menietti, J. D. et al. (2001), Control of Jovian radio emissions by the Galilean moons as observed by Cassini and Galileo, in H. O. Rucker, M. L. Kaiser and Y. Leblanc, eds., *Planetary Radio Emissions V*, pp. 155–64.

Jacobsen, S., Neubauer, F. M., Saur, J. and Schilling, N. (2007), 'Io's nonlinear MHD-wave field in the heterogeneous Jovian magnetosphere', *Geophysical Research Letters* **34**, L10202, doi:https://doi.org/10.1029/2006GL029187.

Jacobsen, S., Saur, J., Neubauer, F. M. et al. (2010), 'Location and spatial shape of electron beams in Io's wake', *Journal of Geophysical Research* **115**(A14), A04205.

Jia, X., Walker, R. J., Kivelson, M. G., Khurana, K. K. and Linker, J. A. (2009), 'Properties of Ganymede's magnetosphere inferred from improved three-dimensional MHD simulations', *Journal of Geophysical Research* **114**, A09209, doi:https://doi.org/10.1029/2009JA014375.

Jia, X., Walker, R. J., Kivelson, M. G., Khurana, K. K. and Linker, J. A. (2008), 'Three-dimensional MHD simulations of Ganymede's magnetosphere', *Journal of Geophysical Research* **113**(A12), 6212.

Jia, X., Walker, R. J., Kivelson, M. G., Khurana, K. K. and Linker, J. A. (2010), 'Dynamics of Ganymede's magnetopause: intermittent reconnection under steady external conditions', *Journal of Geophysical Research: Space Physics* **115**(A14), A12202.

Jones, S. T. and Su, Y.-J. (2008), 'Role of dispersive Alfvén waves in generating parallel electric fields along the Io-Jupiter fluxtube', *Journal of Geophysical Research* **113**(A12), 12205.

Kaiser, M. L. and Alexander, J. K. (1973), 'Periodicities in the Jovian decametric emission', *The Astrophysical Journal Letters* **14**, 55.

Kaiser, M. L. and MacDowall, R. J. (1998), 'Jovian radio "bullseyes" observed by Ulysses', *Geophysical Research Letters* **25**(16), 3113–16.

Kaweeyanun, N., Masters, A. and Jia, X. (2020), 'Favorable conditions for magnetic reconnection at Ganymede's upstream magnetopause', *Geophysical Research Letters* **47**(6), e2019GL086228. eprint: https://agupubs.onlinelibrary.wiley.com/doi/pdf/10.1029/2019GL086228. **URL:** https://agupubs.onlinelibrary.wiley.com/doi/abs/10.1029/2019GL086228.

Khurana, K. K. (1997), 'Euler potential models of Jupiter's magnetospheric field', *Journal of Geophysical Research: Space Physics* **102**(A6), 11295–306. **URL:** https://agupubs.onlinelibrary.wiley.com/doi/abs/10.1029/97JA00563.

Kivelson, M. G. and Bagenal, F. (2014), Chapter 7 – Planetary Magnetospheres, in T. Spohn, D. Breuer and T. V. Johnson, eds., *Encyclopedia of the Solar System* (Third Edition), Elsevier, Boston, pp. 137–57. **URL:** www.sciencedirect.com/science/article/pii/B9780124158450000074.

Kivelson, M. G., Bagenal, F., Kurth, W. S. et al. (2004), Magnetospheric interactions with satellites, in *Jupiter: The Planet, Satellites and Magnetosphere*, pp. 513–36.

Kivelson, M. G., Warnecke, J., Bennett, L. et al. (1998), 'Ganymede's magnetosphere: magnetometer overview', *Journal of Geophysical Research: Planets* **103**(E9), 19963–72. eprint: https://agupubs.onlinelibrary.wiley.com/doi/pdf/10.1029/98JE00227. **URL:** https://agupubs.onlinelibrary.wiley.com/doi/abs/10.1029/98JE00227.

Kurth, W. S., Bolton, S. J., Gurnett, D. A. and Levin, S. (1997a), 'A determination of the source of Jovian hectometric radiation via occultation by Ganymede', *Geophysical Research Letters* **24**(10), 1171–4.

Kurth, W. S., Gurnett, D. A. and Menietti, J. D. (2000), 'The influence of the Galilean satellites on radio emissions from the Jovian system', *Washington DC American Geophysical Union Geophysical Monograph Series* **119**, 213–25.

Kurth, W. S., Gurnett, D. A., Roux, A. and Bolton, S. J. (1997b), 'Ganymede: a new radio source', *Geophysical Research Letters* **24**(17), 2167–70. eprint: https://agupubs.onlinelibrary.wiley.com/doi/pdf/10.1029/97GL02249. **URL:** https://agupubs.onlinelibrary.wiley.com/doi/abs/10.1029/97GL02249.

Lamy, L., Zarka, P., Cecconi, B. et al. (2017), 1977–2017: 40 years of decametric observations of Jupiter and the Sun with the Nancay Decameter Array, in G. Fischer, G. Mann, M. Panchenko and P. Zarka, eds., *Planetary Radio Emissions VIII*, pp. 455–66.

Lavrukhin, A. S. and Alexeev, I. I. (2015), 'Aurora at high latitudes of Ganymede', *Astronomy Letters* **41**(11), 687–92. **URL:** https://doi.org/10.1134/S1063773715110043.

Le Quéau, D. (1988), Planetary radio emissions from high magnetic latitudes: the 'Cyclotron-Maser' theory, in H. O. Rucker, S. J. Bauer and B. M. Pedersen, eds., *Planetary Radio Emissions II*, Austrian Academy of Sciences Press, Graz, Austria, pp. 381–98. **URL:** www.austriaca.at:8080/1523-6inhalt?frames=yes.

Lebo, G. R., Smith, A. G. and Carr, T. D. (1965), 'Jupiter's decametric emission correlated with the longitudes of the first three Galilean satellites', *Science* **148**(3678), 1724–25. **URL:** https://science.sciencemag.org/content/148/3678/1724.

Louis, C. K., Hess, S. L. G., Cecconi, B. et al. (2019), 'ExPRES: an Exoplanetary and Planetary Radio Emissions Simulator', *Astronomy & Astrophysics* **627**, A30.

Louis, C. K., Lamy, L., Zarka, P., Cecconi, B. and Hess, S. L. G. (2017a), 'Detection of Jupiter decametric emissions controlled by Europa and Ganymede with Voyager/PRA and Cassini/RPWS', *Journal of Geophysical Research: Space Physics* **122**(9), 9228–47. eprint: https://agupubs.onlinelibrary.wiley.com/doi/pdf/10.1002/2016JA023779. **URL:** https://agupubs.onlinelibrary.wiley.com/doi/abs/10.1002/2016JA023779.

Louis, C. K., Louarn, P., Allegrini, F., Kurth, W. S. and Szalay, J. R. (2020), 'Ganymede-induced decametric radio emission: in situ observations and measurements by Juno', *Geophysical Research Letters* **47**(20), e2020GL090021. eprint: https://agupubs.onlinelibrary.wiley.com/doi/pdf/10.1029/2020GL090021. **URL:** https://agupubs.onlinelibrary.wiley.com/doi/abs/10.1029/2020GL090021.

Louis, C., Lamy, L., Zarka, P. et al. (2017b), Simulating Jupiter-satellite decametric emissions with ExPRES: a parametric study, in G. Fischer, G. Mann, M. Panchenko and P. Zarka, eds., *Planetary Radio Emissions VIII*, pp. 59–72.

Marques, M. S., Zarka, P., Echer, E. et al. (2017), 'Statistical analysis of 26 yr of observations of decametric radio emissions from Jupiter', *Astronomy & Astrophysics* **604**, A17.

Matsuda, K., Terada, N., Katoh, Y. and Misawa, H. (2012), 'A simulation study of the current-voltage relationship of the Io tail aurora', *Journal of Geophysical Research: Space Physics* **117**(A16), 10214.

Mauk, B. H., Williams, D. J. and McEntire, R. W. (1997), 'Energy-time dispersed charged particle signatures of dynamic injections in Jupiter's inner magnetosphere', *Geophysical Research Letters* **24**(23), 2949–2952. eprint: https://agupubs.onlinelibrary.wiley.com/doi/pdf/10.1029/97GL03026. **URL:** https://agupubs.onlinelibrary.wiley.com/doi/abs/10.1029/97GL03026.

Menietti, J. D., Gurnett, D. A., Kurth, W. S. and Groene, J. B. (1998a), 'Control of Jovian radio emission by Ganymede', *Geophysical Research Letters* **25**(23), 4281–4. eprint: https://agupubs.onlinelibrary.wiley.com/doi/pdf/10.1029/1998GL900112. **URL:** https://agupubs.onlinelibrary.wiley.com/doi/abs/10.1029/1998GL900112.

Menietti, J. D., Gurnett, D. A., Kurth, W. S., Groene, J. B. and Granroth, L. J. (1998b), 'Galileo direction finding of Jovian radio emissions', *Journal of Geophysical Research* **103**(E9), 20001–10.

Moirano, A., Mura, A., Adriani, A. et al. (2021), 'Morphology of the auroral tail of Io, Europa, and Ganymede from JIRAM L-Band Imager', *Journal of Geophysical Research: Space Physics* **126**(9), e2021JA029450. eprint: https://onlinelibrary.wiley.com/doi/pdf/10.1029/2021JA029450. **URL:** https://onlinelibrary.wiley.com/doi/abs/10.1029/2021JA029450.

Moore, K. M., Bloxham, J., Connerney, J. E. P., Jørgensen, J. L. and Merayo, J. M. G. (2017), 'The analysis of initial Juno magnetometer data using a sparse magnetic field representation', *Geophysical Research Letters* **44**, 4687–93.

Mura, A., Adriani, A., Altieri, F. et al. (2017), 'Infrared observations of Jovian aurora from Juno's first orbits: main oval and satellite footprints', *Geophysical Research Letters* **44**, 5308–16.

Mura, A., Adriani, A., Connerney, J. E. P. et al. (2018), 'Juno observations of spot structures and a split tail in Io-induced aurorae on Jupiter', *Science* **361**(6404), 774–7. **URL:** http://science.sciencemag.org/content/361/6404/774.

Neubauer, F. M. (1980), 'Nonlinear standing Alfven wave current system at Io - Theory', *Journal of Geophysical Research* **85**, 1171–8.

Neubauer, F. M. (1998), 'The sub-Alfvénic interaction of the Galilean satellites with the Jovian magnetosphere', *Journal of Geophysical Research: Planets* **103**(E9), 19843–66. eprint: https://agupubs.onlinelibrary.wiley.com/doi/pdf/10.1029/97JE03370. **URL:** https://agupubs.onlinelibrary.wiley.com/doi/abs/10.1029/97JE03370

Paranicas, C., Mauk, B. H., Haggerty, D. K. et al. (2019), 'Io's effect on energetic charged particles as seen in Juno data', *Geophysical Research Letters* **46**(23), 13615–20. eprint: https://agupubs.onlinelibrary.wiley.com/doi/pdf/10.1029/2019GL085393. **URL:** https://agupubs.onlinelibrary.wiley.com/doi/abs/10.1029/2019GL085393.

Pryor, W. R., Rymer, A. M., Mitchell, D. G. et al. (2011), 'The auroral footprint of Enceladus on Saturn', *Nature* **472**(7343), 331–3. **URL:** www.nature.com/articles/nature09928.

Saur, J., Grambusch, T., Duling, S., Neubauer, F. M. and Simon, S. (2013), 'Magnetic energy fluxes in sub-Alfvénic planet star and moon planet interactions', *Astronomy & Astrophysics* **552**, A119. **URL:** www.aanda.org/articles/aa/abs/2013/04/aa18179-11/aa18179-11.html.

Saur, J., Neubauer, F. M., Connerney, J. E. P., Zarka, P. and Kivelson, M. G. (2004), Plasma interaction of Io with its plasma torus, in *Jupiter. The Planet, Satellites and Magnetosphere*, pp. 537–60. Citation Key Alias: saurPlasmaInteractionsIo.

St. Cyr, O. C. (1985), Jupiter's decameter and kilometer emissions: satellite effects and long term periodicities, PhD thesis, University of Florida, Gainesville.

Su, Y.-J., Ergun, R. E., Bagenal, F. and Delamere, P. A. (2003), 'Io-related Jovian auroral arcs: Modeling parallel electric fields', *Journal of Geophysical Research: Space Physics* **108**(A2). **URL:** https://agupubs.onlinelibrary.wiley.com/doi/abs/10.1029/2002JA009247.

Sulaiman, A. H., Hospodarsky, G. B., Elliott, S. S. et al. (2020), 'Wave-particle interactions associated with Io's auroral footprint: evidence of Alfvén, ion cyclotron, and whistler modes', *Geophysical Research Letters* **47**(22), e2020GL088432. eprint: https://agupubs.onlinelibrary.wiley.com/doi/pdf/10.1029/2020GL088432. **URL:** https://agupubs.onlinelibrary.wiley.com/doi/abs/10.1029/2020GL088432.

Szalay, J. R., Allegrini, F., Bagenal, F. et al. (2020a), 'Alfvénic acceleration sustains Ganymede's footprint tail aurora', *Geophysical Research Letters* **47**(3), e2019GL086527. eprint: https://agupubs.onlinelibrary.wiley.com/doi/pdf/10.1029/2019GL086527. **URL:** https://agupubs.onlinelibrary.wiley.com/doi/abs/10.1029/2019GL086527.

Szalay, J. R., Bagenal, F., Allegrini, F. et al. (2020b), 'Proton acceleration by Io's Alfvénic interaction', *Journal of Geophysical Research: Space Physics* **125**(1), e2019JA027314. eprint: https://agupubs.onlinelibrary.wiley.com/doi/pdf/10.1029/2019JA027314. **URL:** https://agupubs.onlinelibrary.wiley.com/doi/abs/10.1029/2019JA027314.

Szalay, J. R., Bonfond, B., Allegrini, F. et al. (2018), 'In situ observations connected to the Io footprint tail aurora', *Journal of Geophysical Research: Planets* **123**(11), 3061–77. **URL:** https://agupubs.onlinelibrary.wiley.com/doi/abs/10.1029/2018JE005752.

Vogt, M. F., Bunce, E. J., Kivelson, M. G. et al. (2015), 'Magnetosphere-ionosphere mapping at Jupiter: quantifying the effects of using different internal field models', *Journal of Geophysical Research: Space Physics* **120**(4), 2584–99. **URL:** https://agupubs.onlinelibrary.wiley.com/doi/abs/10.1002/2014JA020729.

Vogt, M. F., Kivelson, M. G., Khurana, K. K. et al. (2011), 'Improved mapping of Jupiter's auroral features to magnetospheric sources', *Journal of Geophysical Research: Space Physics* **116**, A03220, doi:https://doi.org/10.1029/2010JA016148. **URL:** https://agupubs.onlinelibrary.wiley.com/doi/full/10.1029/2010JA016148.

Wannawichian, S., Clarke, J. T. and Nichols, J. D. (2010), 'Ten years of Hubble Space Telescope observations of the variation of the Jovian satellites' auroral footprint brightness', *Journal of Geophysical Research: Space Physics* **115**, A02206, doi:https//doi.org/10.1029/2009JA014456. **URL:** https://agupubs.onlinelibrary.wiley.com/doi/abs/10.1029/2009JA014456.

Williams, D. J. and Mauk, B. (1997), 'Pitch angle diffusion at Jupiter's moon Ganymede', *Journal of Geophysical Research* **102**(A11), 24283–302.

Williams, D. J., Mauk, B. H., McEntire, R. W. et al. (1997), 'Energetic particle signatures at Ganymede: implications for Ganymede's magnetic field', *Geophysical Research Letters* **24**(17), 2163–6.

Yoneda, M., Kagitani, M. and Okano, S. (2009), 'Short-term variability of Jupiter's extended sodium nebula', *Icarus* **204**(2), 589–96. **URL:** www.sciencedirect.com/science/article/pii/S0019103509003157.

Yoneda, M., Tsuchiya, F., Misawa, H. et al. (2013), 'Io's volcanism controls Jupiter's radio emissions', *Geophysical Research Letters* **40**(4), 671–5. **URL:** https://agupubs.onlinelibrary.wiley.com/doi/abs/10.1002/grl.50095.

Zarka, P. (1998), 'Auroral radio emissions at the outer planets: observations and theories', *Journal of Geophysical Research: Planets* **103**(E9), 20159–94. **URL:** https://agupubs.onlinelibrary.wiley.com/doi/abs/10.1029/98JE01323.

Zarka, P. (2007), 'Plasma interactions of exoplanets with their parent star and associated radio emissions', *Planetary and Space Science* **55**(5), 598–617.

Zarka, P. (2020), Star-planet interactions in the radio domain: prospect for their detection, in H. J. Deeg and J. A. Belmonte, eds., *Handbook of Exoplanets*, Springer International Publishing, Cham, pp. 1–16. **URL:** https://doi.org/10.1007/978-3-319-30648-3_22-2.

Zarka, P., Marques, M. S., Louis, C. et al. (2018), 'Jupiter radio emission induced by Ganymede and consequences for the radio detection of exoplanets', *Astronomy & Astrophysics* **618**, A84. **URL:** www.aanda.org/articles/aa/abs/2018/10/aa33586-18/aa33586-18.html.

Zarka, P., Treumann, R. A., Ryabov, B. P. and Ryabov, V. B. (2001), 'Magnetically-driven planetary radio emissions and application to extrasolar planets', *Astrophysics and Space Science* **277**, 293–300.

Zhou, H., Tóth, G., Jia, X. and Chen, Y. (2020), 'Reconnection-driven dynamics at Ganymede's upstream magnetosphere: 3-D Global Hall MHD and MHD-EPIC simulations', *Journal of Geophysical Research: Space Physics* **125**(8), e28162.

Zhou, H., Tóth, G., Jia, X., Chen, Y. and Markidis, S. (2019), 'Embedded kinetic simulation of Ganymede's magnetosphere: improvements and inferences', *Journal of Geophysical Research: Space Physics* **124**(7), 5441–60.